Extended Data Figure 1: Receptor constructs, T cell generation and gene editing

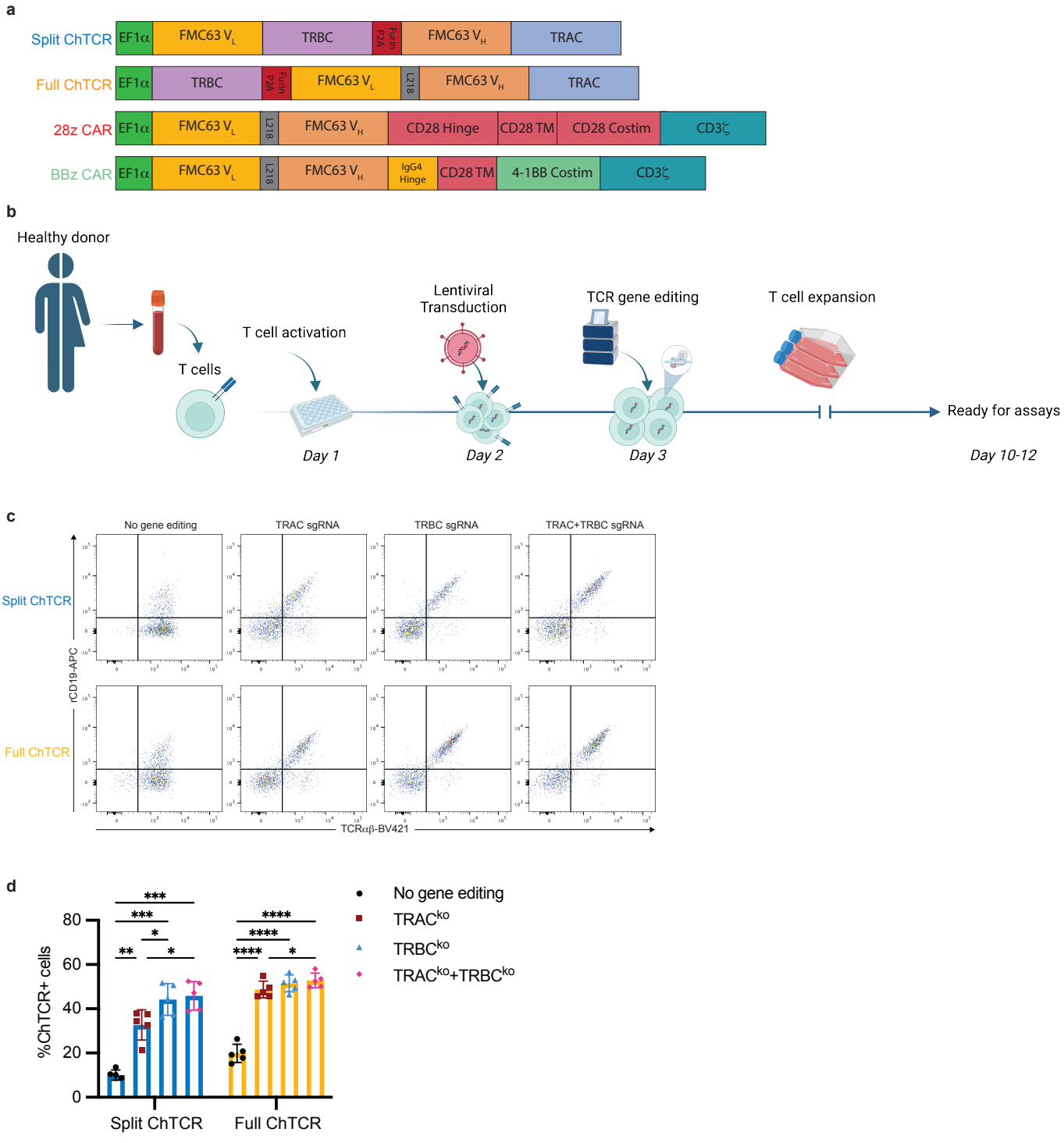

Extended Data Figure 2: ChTCRs assemble with all CD3 subunits in primary T cells

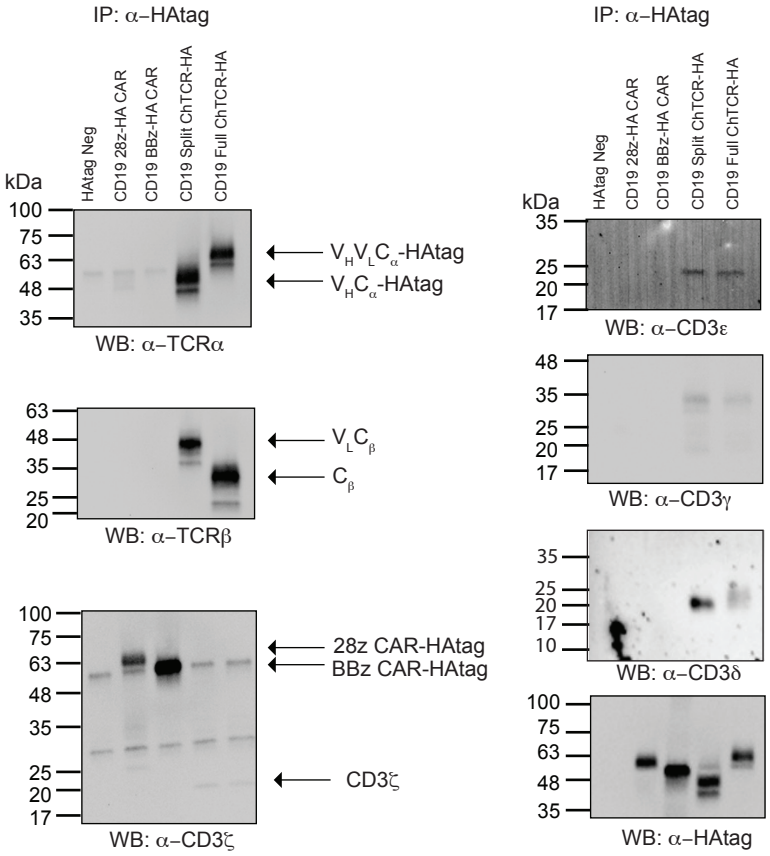

Extended Data Figure 3: CD19-specific ChTCRs lack tonic signaling in Jurkat TPR reporter cells.

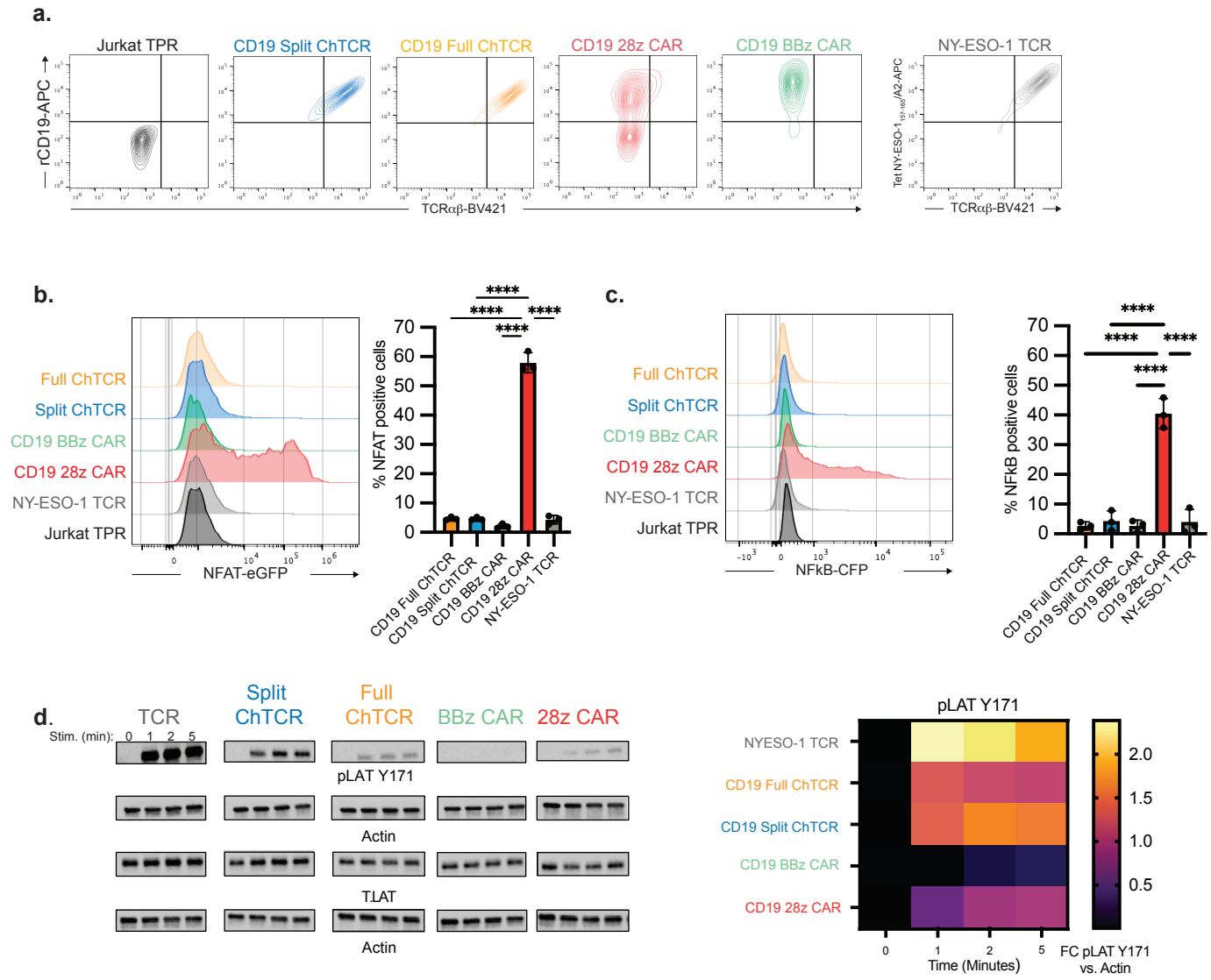

Extended Data Figure 4. TRAC usage does not improve m971-based ChTCR T cell functions

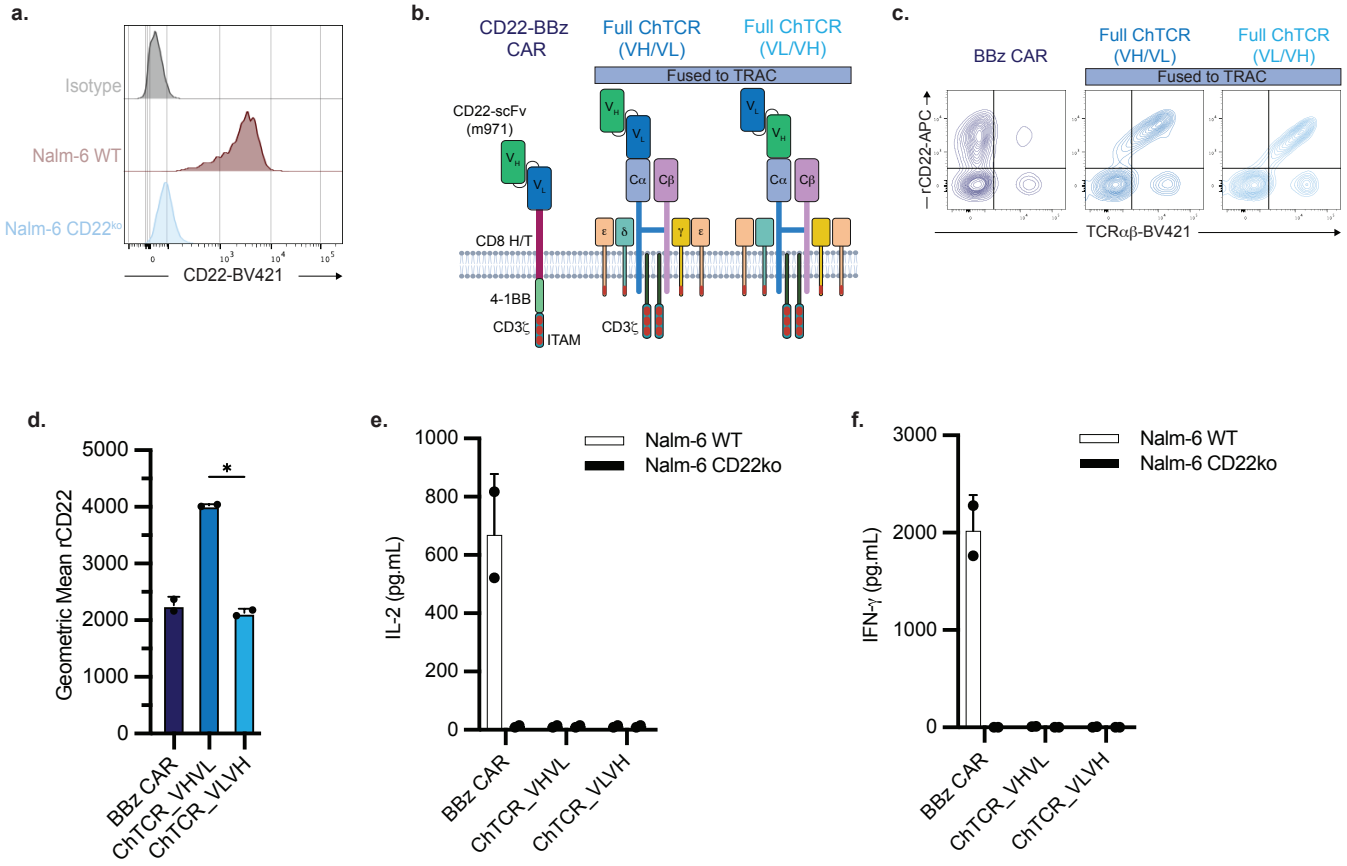

Extended Data Figure 5. T cells expressing the CD22-specific Full ChTCR demonstrate superior antigen sensitivity

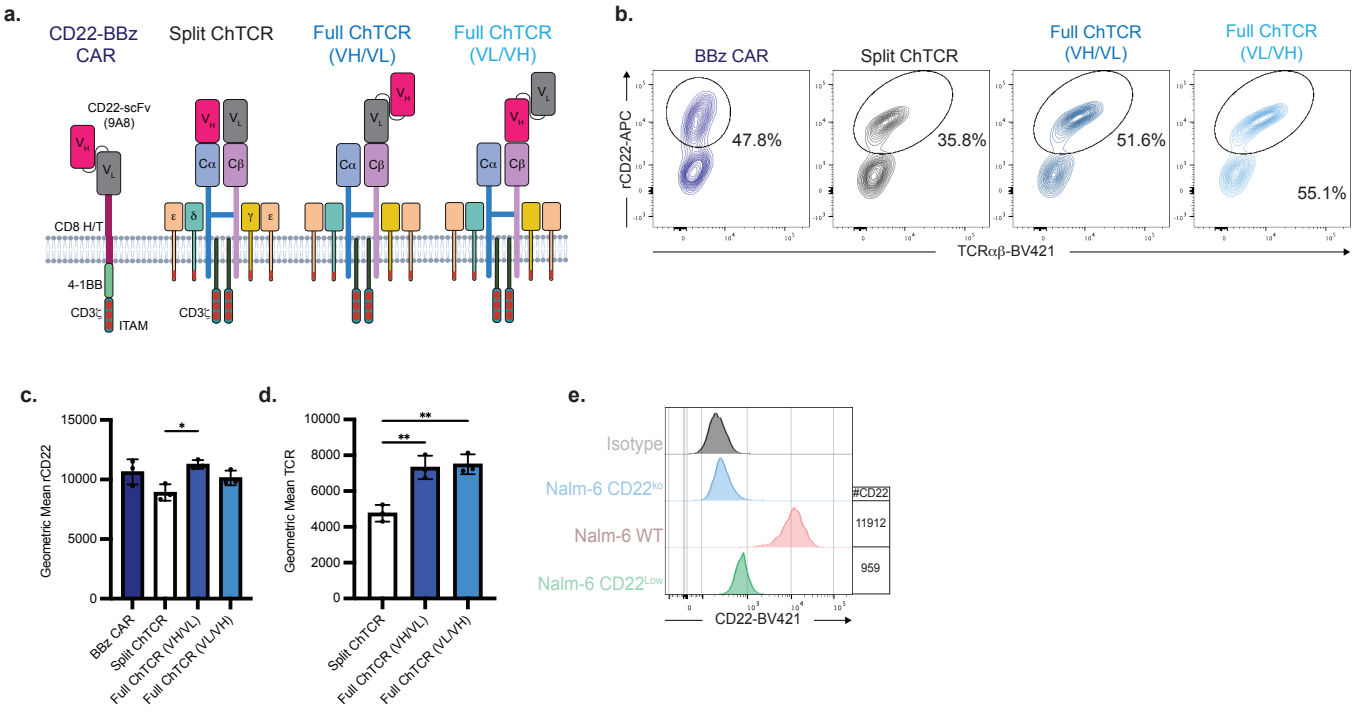

Extended data Figure 6. Design and function of bispecific CD19/CD22 ChTCR

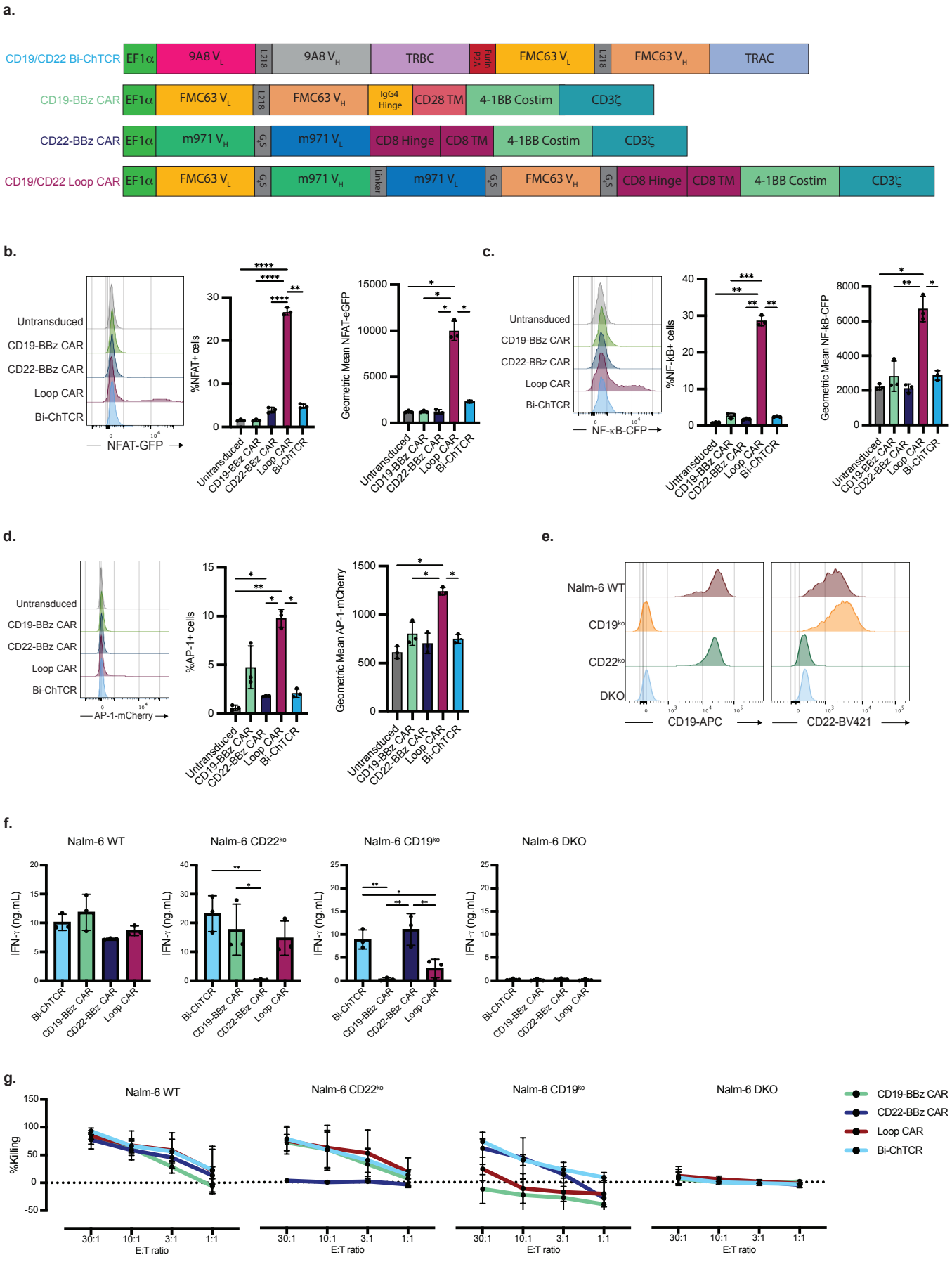

Extended Data Figure 7. Optimizing design of BCMA/SLAMF7 Bi-ChTCRs

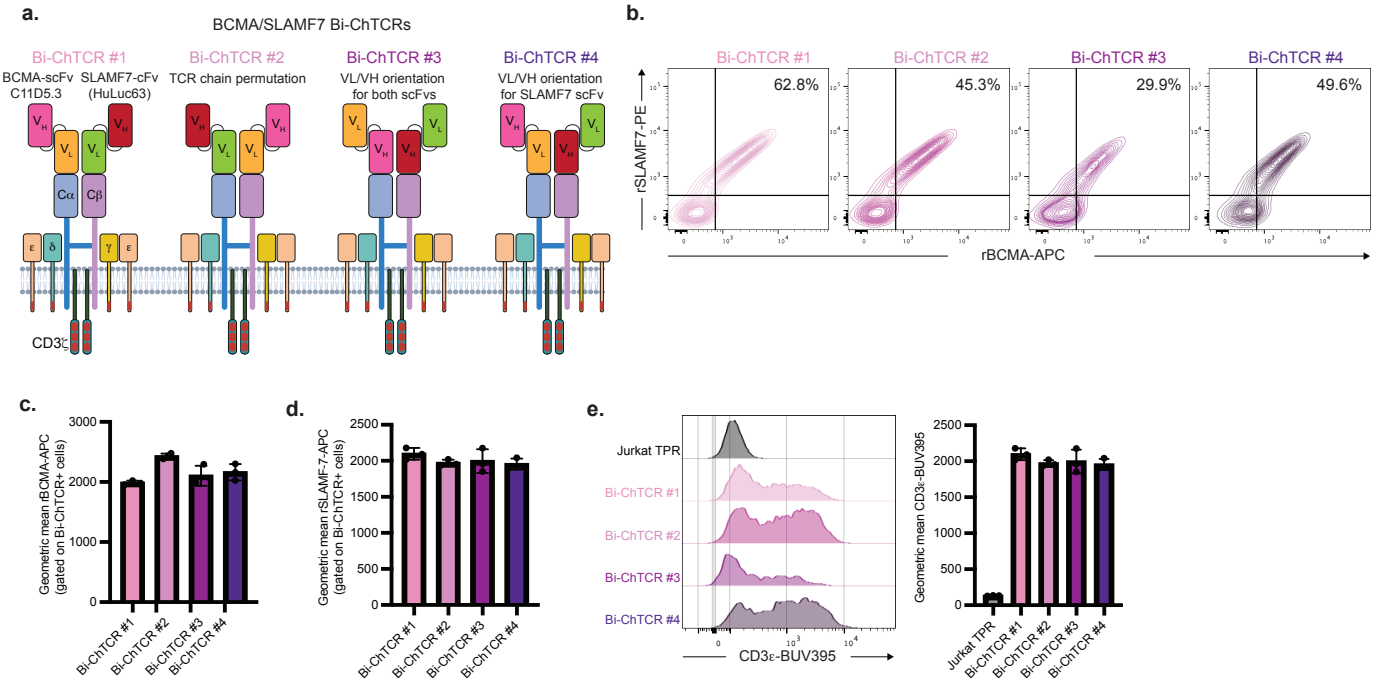

Extended Data Figure 8: BCMA/SLAMF7 receptor constructs, SLAMF7 gene editing, and antigen sensitivity of BCMA/SLAMF7 bi-ChTCR T cells.

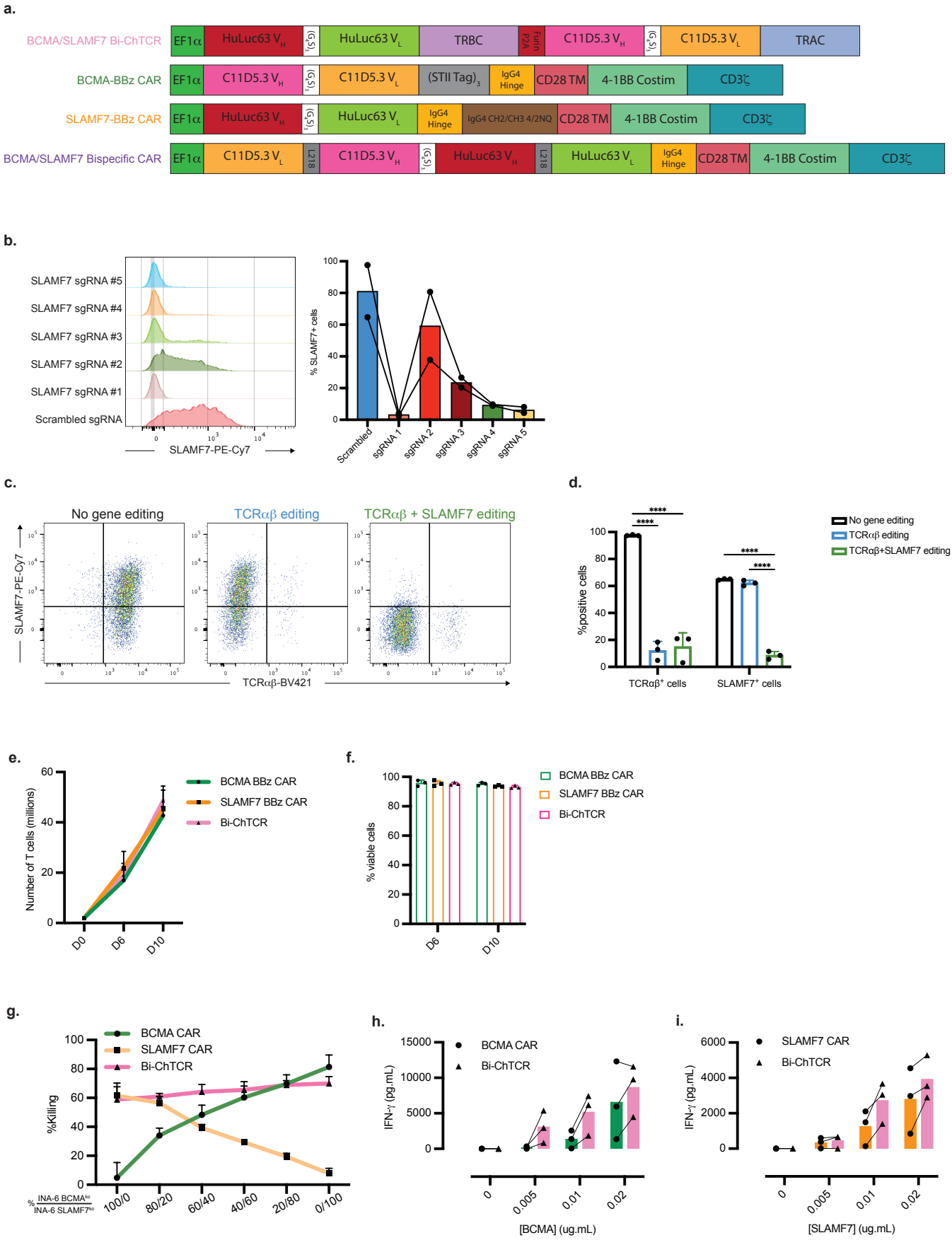

Extended Data Figure 9: T cells expressing the BCMA/SLAMF7 Bi-ChTCR are superior to a bispecific CAR for antigen binding and proximal signaling.

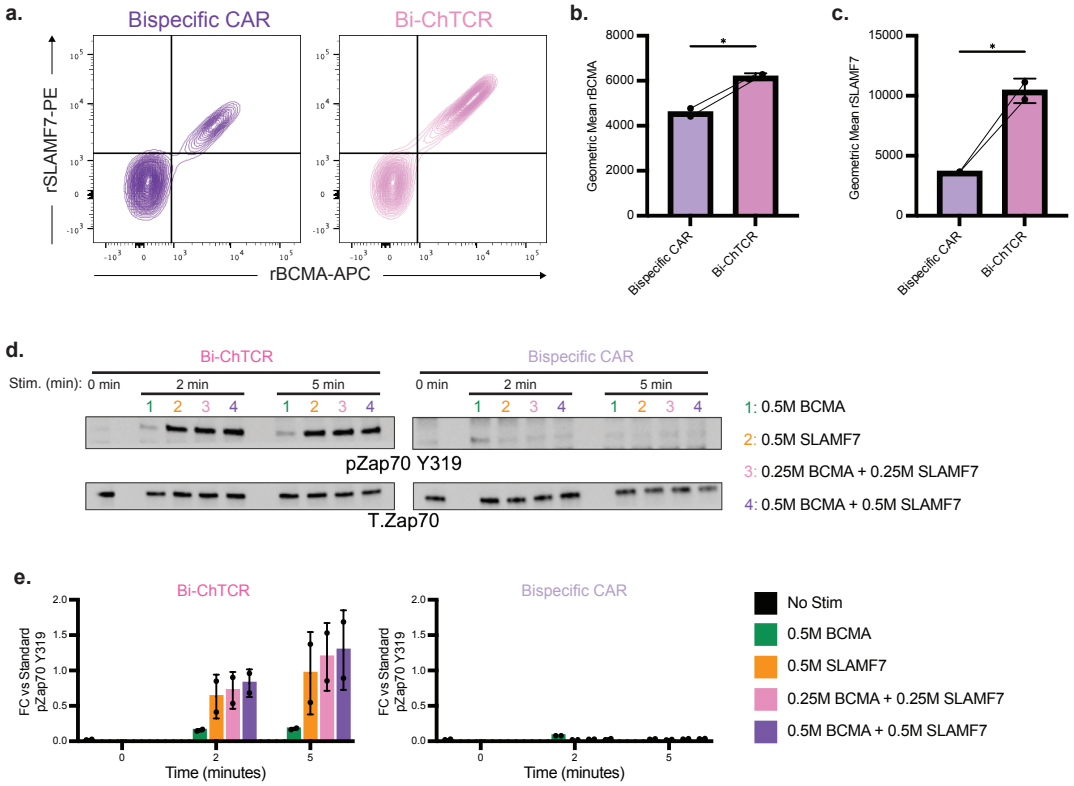

Extended Data Figure 1. Receptor constructs, T cell generation and gene editing

a. Schematic of CD19-specific ChTCR and CAR receptor constructs. **b.** CAR and ChTCR transduction and cytosine base editing of TCR$\alpha\beta$ genes primary T cells. **c.** Representative flow cytometry plots of ChTCR T cells stained with TCR-BV421 and recombinant CD19 protein-APC without TCR knockout, after single TRAC KO, single TRBC KO or double TRAC and TRBC KO. **d.** Frequency of ChTCR$^+$ T cells without and with knockout of TRAC, TRBC or both. Data is shown as the mean $\pm$ SD for 5 independent experiments. *P<0.05, **P<0.01, ***P<0.001 and ****P<0.0001 by two-way ANOVA.

Extended Data Figure 2. ChTCRs assemble with all CD3 subunits in primary T cells

Western blot analysis of TCRα, TCRβ and CD3ζ, δ, ε and γ subunits following immunoprecipitation of HA-tagged CAR and ChTCR receptors from transduced and gene edited primary T cell using and anti-HA tag antibody. Cell expressing a TCR receptor without an HA tag was used as a negative control. Proteins co-immunoprecipitated with each of the receptors were detected by western blot with antibodies specific to TCRα, TCRβ and each of the CD3 subunits. Blotting with anti-HA was performed as a loading/immunoprecipitation control.

Extended Data Figure 3. CD19-specific ChTCRs lack tonic signaling in Jurkat TPR reporter cells.

a. Representative flow plots showing expression of CD19-specific ChTCRs and CARs (TCR$\alpha\beta$-BV421 and recombinant CD19-APC) and NY-ESO-1-specific TCR 1G4 (TCR$\alpha\beta$-BV421 and NY-ESO-$1_{157\text{-}165}$/A2 tetramer-APC) in Jurkat 76 TPR cells. **b.** Left: Representative histogram of NFAT-eGFP reporter expression in J76 TPR Jurkat cells expressing the indicated receptors. Right: Mean frequency $\pm$ SD of NFAT-eGFP positive cells (n=3 independent experiments). ****P<0.0001 by two-way ANOVA. **c.** Left: Representative histogram of NFκB-CFP reporter expression in J76 TPR Jurkat cells expressing the indicated receptors. Right: Mean frequency $\pm$ SD of NFκB-CFP positive cells (n=3 independent experiments). ****P<0.0001 by two-way ANOVA. **d.** Left: Representative western blot analysis for LAT pTyr^{171}, Actin and LAT. Right: Heat map of mean band intensity of LAT pTyr^{171} normalized to actin loading control (n=2 independent experiments).

Extended Data Figure 4: TRAC usage does not improve m971-based ChTCR T cell functions.

a. CD22 expression measured by flow cytometry on Nalm-6 WT or CD22^{ko}. **b.** Schematic of anti-CD22 CAR and Full ChTCRs using m971 scFv in VH/VL or VL/VH orientation fused to TRAC. **c.** Representative flow plots showing expression of CD22-specific CAR and Full ChTCRs in primary CD8+ T cells (TCRα/β-BV421 and rCD22-APC). **d.** Geometric mean $\pm$ SD of rCD22-protein-APC bound to receptors (n=2 independent experiments). *P<0.05 by two-way ANOVA. **e. and f.** Concentration of IL-2 (e) or IFN-γ (f) in culture supernatant after overnight co-culture of CAR and ChTCR T cells with the indicated Nalm-6 cells (mean $\pm$ SD, n=2 independent experiments).

Extended Data Figure 5. T cells expressing the CD22-specific Full ChTCR demonstrate superior antigen sensitivity.

a. Schematic of CD22-specific CAR, Split ChTCR and Full ChTCRs using 9A8 scFv. **b.** Representative flow plots of CAR and ChTCR expression on primary CD8 T cells stained with TCR$\alpha\beta$-BV421 and recombinant CD22-protein-APC. **c.** Geometric mean $\pm$ SD of recombinant CD22-protein-APC bound to CD22-specific receptors (n=3 independent experiments). *P<0.05 by two-way ANOVA. **d.** Geometric mean $\pm$ SD of TCR$\alpha\beta$-BV421 expression by CD22-specific ChTCRs (n=3 independent experiments). **P<0.01 by two-way ANOVA. **e**. CD22 expression by Nalm-6 WT, $CD22^{ko}$ and $CD22^{Low}$ target cells measured by flow cytometry.

Extended Data Figure 6: Design and function of bispecific CD19/CD22 ChTCR

a. Schematic of CD19- and CD22- mono- and bispecific receptor constructs. **b-d.** Left: Representative histograms of NFAT-GFP (b), NFκB-CFP (c) and AP-1-mCherry (d) reporter expression in J76 TPR Jurkat cells expressing the indicated receptors. Middle: Frequency of NFAT-GFP (b), NFκB-CFP (c) and AP-1-mCherry (d) positive cells. Right: Geometric mean $\pm$ SD of NFAT-GFP (b), NFκB-CFP (c) and AP-1-mCherry (d) reporter genes (n=3 independent experiments). *P<0.5, **P<0.01, *** P<0.001, ****P<0.0001 by two-way ANOVA. **e.** CD19 and CD22 expression by Nalm-6 WT, $CD19^{+}CD22^{ko}$, $CD19^{ko}CD22^{+}$ and $CD19^{ko}CD22^{ko}$ target cells measured by flow cytometry. **f.** Concentration of IFN-γ in culture supernatant after overnight co-culture of T cells expressing the indicated CARs and Bi-ChTCRs with indicated Nalm-6 cell lines. Data is shown as the mean $\pm$ SD for 3 independent experiments. *P<0.05 and **P<0.01 by two-way ANOVA. **g.** Cytotoxicity of the indicated Nalm-6 cell lines by CAR and Bi-ChTCR T cells at varying E:T ratios.

Extended Data Figure 7: Optimizing design of BCMA/SLAMF7 Bi-ChTCRs

a. Schematic of BCMA/SLAMF7 Bi-ChTCR receptors with different configurations of VH/VL and linkage to TCR chains. **b.** Representative flow plots of Jurkat 76 TPR cells expressing the indicated Bi-ChTCR receptors after staining recombinant SLAMF7 and BCMA protein. **c. and d.** Geometric mean $\pm$ SD of rBCMA-PE (c) and rSLAMF7-APC (d) bound to receptors (gated on Bi-ChTCR+ cells; n=3 independent experiments). **e.** Right: Representative histogram of CD3ε expression in Bi-ChTCR+ and Jurkat TPR cells. Right: Geometric mean $\pm$ SD of CD3ε expression (gated on Bi-ChTCR+ cells; n=3 independent experiments).

Extended Data Figure 8: BCMA/SLAMF7 receptor constructs, SLAMF7 gene editing, and antigen sensitivity of BCMA/SLAMF7 bi-ChTCR T cells.

a. Schematic of SLAMF7- and BCMA- mono- and bispecific receptor constructs. **b.** Left: Representative flow histograms of SLAMF7 expression on primary CD8 T cells KO for SLAMF7 using CBE and 5 different SLAMF-7 specific sgRNAs. Right: Frequency of SLAMF7+ cells after

gene editing (n=2 independent experiments). **c.** Representative flow plots of CD8 primary T cells edited or not for TRAC and TRBC and/or SLAMF7. **d**. Frequency ± SD of TCR$\alpha\beta$ and SLAMF7+ cells after TRAC and TRBC KO with or without concomitant SLAMF7 KO (n=3 independent experiments). ***P<0.001 and ****P<0.0001 by two-way ANOVA. **e.** Absolute numbers ± SD of BCMA and SLAMF7 CAR and Bi-ChTCR T cells. **f**. Viability ± SD of BCMA and SLAMF7 CAR and Bi-ChTCR T cells (n=3 independent experiments). **g.** Cytotoxicity assay of CAR and Bi-ChTCR T cells using different ratios of Nalm-6 SLAMF7^{+}BCMA^{-} and SLAMF7^{-}BCMA^{+} tumor cells to mimic antigen heterogeneity (Data is shown as the mean ± SD at an E:T of 10:1, n=3 independent experiments). **h. and i.** INF-γ production (pg/mL) of CAR and Bi-ChTCR to various concentrations of plate bound recombinant BCMA protein (h.) or recombinant SLAMF7 protein (i.) (n=3 independent experiments).

Extended Data Figure 9: T cells expressing the BCMA/SLAMF7 Bi-ChTCR are superior to a bispecific CAR for antigen binding and proximal signaling.

a. Representative flow plots showing binding of recombinant BCMA-APC and SLAMF7-PE to primary CD8 T cells transduced with the BCMA/SLAMF7 bispecific CAR and Bi-ChTCR. **b. and c.** Geometric mean ± SD of rBCMA-APC (b.) and rSLAMF7-PE binding to bispecific CAR and bi-ChTCR T cells (c.) (gated on receptor positive cells; n=2 independent experiments). **d.** Representative western blot analysis for pZap70 pTyr^{319} and Zap70 for Bi-ChTCR or bispecific CAR stimulated with 0.5M of rBCMA (1), 0.5M of rSLAMF7 (2), 0.25M of rBCMA + 0.25M rSLAMF7 (3) or .05M rBCMA + 0.5M rSLAMF7 (4) coated-beads for indicated time. **e.** Mean band intensity ± SD for pZap70 pTyr^{319} normalized to standard (n=2 independent experiments).